Note after first publication:

The originally published version of this Supplementary Information, available online from 23rd January 2025 to 20th February 2025, did not display Figures S1-S3, S5-S13 and S16 due to a technical issue with a conversion of the original Word document to PDF. As of 20/02/2025, the supplementary information has been updated to the version that was submitted during the final round of peer review. The Royal Society of Chemistry apologises to the authors and readers for any inconvenience caused. Ellis Crawford, Scientific Editor, 20/02/2025.

Efficient harvesting of triplet excitons by fast TTA up-conversion and highly-lying reverse intersystem crossing multi-channels for efficient blue fluorescent organic light-emitting diodes

Jianwen Qin, Xianfeng Qiao*, Shu Xiao, Dezhi Yang, Yanfeng Dai, Jiangshan Chen, Qian Sun and Dongge Ma*

Institute of Polymer Optoelectronic Materials and Devices, Guangdong Basic Research Center of Excellence for Energy & Information Polymer Materials, Guangdong-Hong Kong-Macao Joint Laboratory of Optoelectronic and Magnetic Functional Materials, Guangdong Provincial Key Laboratory of Luminescence from Molecular Aggregates, State Key Laboratory of Luminescent Materials and Devices, South China University of Technology, Guangzhou 510640, China

E-mail: msdgma@scut.edu.cn, msxqiao@scut.edu.cn

1. Material characterization

The UV-vis absorption spectra were measured on a Shimadzu UV-2600 spectrophotometer. The PL spectra were recorded on a Horiba Fluoromax-4 spectrofluorometer. The transient PL spectra were detected by Edinburgh Instrument FLS980 with the pulse excitation wavelength of 370 nm. The fluorescence quantum yields were measured using a Hamamatsu absolute PL quantum yield spectrometer C11347 Quantaurus_QY. The HOMO energy level was determined from the onset

potential of oxidation by cyclic voltammetry [HOMO = − (E_{onset} + 4.4)], and LUMO energy level was deduced from HOMO and optical band gap (E_g) (LUMO = HOMO + E_g). The ground state geometries were optimized using the density function theory (DFT) method with B3LYP hybrid functional at the basis set level of 6-31G (d). All the calculations were performed using Gaussian 09 package.

2. Device fabrication and characterization

All the organic materials used in experiments were purchased from Lumtec, Inc. All compounds were subjected to temperature-gradient sublimation under high vacuum before used. The OLEDs were fabricated on ITO-coated glass substrates with multiple organic layers sandwiched between the transparent bottom indium-tin-oxide (ITO) anode and the top metal cathode. The clean ITO substrates had a sheet resistance of 10 Ω per square with an emission area of 4×4 mm^2. Before being transferred into vacuum chamber, the dried ITO substrates were treated with UV/ozone for 15 min. The devices were fabricated when the pressure of vacuum chamber was below 5×10^{-4} Pa. And the organic layers were deposited onto the ITO substrates at the rate of 0.1–0.2 nm s^{-1}. A LiF layer with a thickness of 1 nm was deposited on organic layers with a rate of 0.01 nm s^{-1} for improving electron injection. And then, an Al layer as the cathode was deposited by a rate of 0.3 nm s^{-1}. The current density–luminance–voltage characteristics were measured by Keithley 2400 and Luminance Meter LS-110. The EL spectra were tested by an optical analyzer, FlAME-S-VIS-NIR. The external quantum efficiencies were calculated by assuming devices as Lambertian light sources. All the device measurements were carried out under the ambient laboratory conditions.

3. Material synthesis

All the chemicals, reagents, and solvents were purchased from commercial sources and used as received without further purification, unless otherwise mentioned. The column chromatography was carried out on silica gel (200-300 mesh). The ^{1}H NMR spectra were measured using Bruker Avance 500 MHz. Additionally, the high resolution mass spectra were performed using JEOL JMS-600W Gas Chromatography-Mass spectrometer. The starting materials and solvents were purchased from Aldrich Chemical Co., or Energy Chemical Co., China. The toluene was distilled over metallic sodium before use. They were used without further purification.
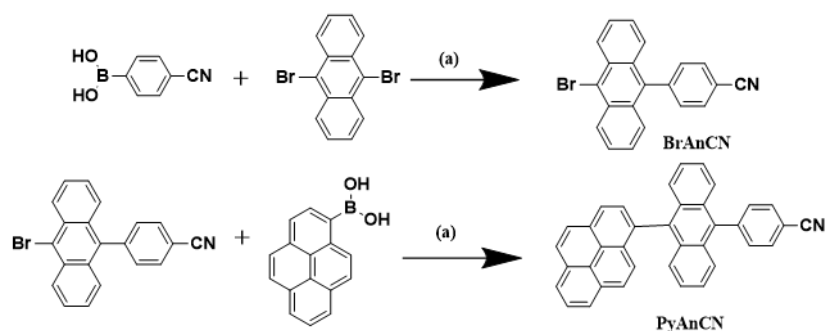
Scheme S1. Synthetic procedures. (a) Pd(PPh₃)₄, K₂CO₃, toluene and water, 90 °C, 12 hours under N₂ atmosphere. The synthesis of BrAnCN were performed according to previous reports.[1]

Synthesis of 4-(10-(pyren-1-yl)anthracen-9-yl)benzonitrile (**PyAnCN**):

In a 100 mL round flask, a mixture of BrAnCN (1.79 g, 5 mmol), Pyrene-1-boronic acid (1.23 g, 5 mmol), K₂CO₃ (5.52 g, 40 mmol), 20 mL distilled water, 40 mL toluene and Pd(PPh₃)₄ (115 mg, 0.10 mmol) were added, the solution refluxed at 90 °C under nitrogen atmosphere for 12 hours. The mixture was poured into water to quench the reaction and then extracted with dichloromethane, the organic phase was collected and dried over anhydrous Na₂SO₄. After evaporation of the solvent, the residue was purified via column chromatography by using petroleum ether/dichloromethane (2:1, v/v) as eluent to afford yellow solid. (1.12 g, yield: 47%). ¹H NMR (500 MHz, Chloroform-d): δ 8.41 (d, J = 7.7 Hz, 1H), 8.30 – 8.17 (m, 3H), 8.14 (dd, J = 7.7, 1.1 Hz, 1H), 8.09 – 8.00 (m, 2H), 7.97 (td, J = 8.9, 1.7 Hz, 2H), 7.83 (d, J = 9.2 Hz, 1H), 7.79 – 7.73 (m, 1H), 7.74 – 7.67 (m, 1H), 7.64 (dt, J = 8.9, 1.0 Hz, 2H), 7.45 – 7.34 (m, 5H), 7.22 (ddd, J = 8.8, 6.4, 1.2 Hz, 2H). ¹³C NMR (Chloroform-d): δ 144.53, 136.65, 135.01, 133.64, 132.39, 132.36, 131.45, 131.21, 131.02, 130.84, 130.79, 129.48, 129.29, 127.91, 127.83, 127.47, 127.45, 126.22, 126.17, 125.84, 125.56, 125.48, 125.42, 125.27, 124.77, 118.93, 111.71. MS (mass m/z): calculated for C₃₇H₂₁N, 479.58; found, 479,72.

4. Photophysical Equations

The rate constants are determined using the following equations[2]:

$$R_p = \frac{A_1 t_1}{A_1 t_1 + A_2 t_2} \tag{1}$$

$$R_d = \frac{A_2 t_2}{A_1 t_1 + A_2 t_2} \tag{2}$$

$$\varphi_p = \varphi_{PL} R_p \tag{3}$$

$$\varphi_d = \varphi_{PL} R_d \qquad (4)$$

$$k_p = \frac{1}{\tau_p} = \frac{1}{t_1} \qquad (5)$$

$$k_d = \frac{1}{\tau_d} = \frac{1}{t_2} \qquad (6)$$

$$k_S = \frac{\varphi_{PL}}{\tau_p} \qquad (7)$$

$$k_{NR,S} = \frac{k_S}{\varphi_{PL}} - k_S \qquad (8)$$

$$k_{hISC} = (1 - \varphi_p)k_p \qquad (9)$$

$$k_{hRISC} = \frac{k_p k_d \varphi_d}{k_{hISC}\varphi_p} \qquad (10)$$

Here φ_{PL} is the photoluminescence quantum yield (PLQY). φ_p and φ_d are the prompt and delayed fluorescence efficiencies, respectively. k_{hISC} and k_{hRISC} are the hISC and hRISC rates, respectively. τ_p and τ_d are the prompt and delayed fluorescent lifetimes, respectively. k_S, k_{NR}, k_{hISC}, k_{hRISC}, k_p and k_d are the rates of singlet radiation, singlet non-radiation, hISC, hRISC, prompt fluorescence and decay fluorescence processes, respectively. R_p and R_d are the component ratios of prompt and delayed fluorescence, respectively.

5. Steady-state Kinetic Equation

It is assumed that singlet and triplet excitons are directly formed on TTA molecules. The triplet excitons can indirectly generate EL through TTA up-conversion process, together with the direct EL from the singlet excitons. The dynamics can be described by the following three coupled rate equations:

$$\frac{de}{dt} = \frac{dh}{dt} = \frac{J}{qd} - keh \qquad (1)$$

$$\frac{dS}{dt} = P_s keh - (k_S + k_{NR,S})S + \frac{f_1}{2} k_{TT}TT \qquad (2)$$

$$\frac{dT}{dt} = (1 - P_s)keh - (k_{TT}T + k_{NR,T})T \qquad (3)$$

Where e, h, S and T are the densities of electrons, holes, singlets, and triplets in EML, respectively. P_s is the ratio of excitons converting to singlets. k_S and $k_{NR,S}$ represent the rate constants of singlet radiative transition and singlet nonradiative transition, respectively. $k_{NR,T}$ is the rate constant of non-radiative triplet decay. k_{TT} is the rate constant of TTA up-conversion between T and T. k is the Langevin recombination rate. q is the elementary charge. d is the width of the recombination zone.

f_l represents the ratio of TTA up-conversion to singlets. The solution to equation (1) - (3) is a bi-exponential decay given by

$$S = Ae^{-k_p t} + Be^{-k_d t} \tag{4}$$

At high current density and thus high exciton density, where bimolecular TTA up-conversion becomes dominant, the decay lifetime depends on the rate of non-radiative triplet decay, and $k_d = 2k_{NR,T}$.

At low current density, the triplets are difficult to encounter others during the whole lifetime. The monomolecular decay dominates and the bimolecular TTA up-conversion can be neglected ($k_{NR,T} \gg k_{TT}T$).

The singlet density as a function of the current obeys the following expression

$$S = \frac{P_s J}{(k_S + k_{NR})qd} + \frac{f_1 k_{TT}(1 - P_s)^2 J^2}{2k_T^2(k_S + k_{NR})q^2 d^2} \tag{5}$$

At high current density and thus high excitons density, where bimolecular TTA up-conversion becomes dominant ($k_{NR,T} \ll k_{TT}T$), the expression for singlets is then given by

$$S = \frac{P_s J}{(k_S + k_{NR})qd} + \frac{f_1(1 - P_s)J}{2(k_S + k_{NR})qd} \tag{6}$$

The first part is the singlets from the direct charge recombination on TTA molecules, and the second part is the singlets indirectly produced via TTA up-conversion, which are proportional to the square of the current density at low current density (equation (5)), and become linear at high current density (equation (6)). Since the EL intensity is proportional to the singlet density, the ratio R of the EL intensity from the two parts can be determined.

At low current density

$$R = \frac{EL_T}{EL_S} = \frac{f_1 k_{TT}(1 - P_s)^2 J}{2k_{NR,T}^2 qdP_s} \tag{7}$$

$$EQE = \frac{k_S S \eta_{out}}{\frac{J}{qd}} = \varphi_{PL}\eta_{out}(P_S + \frac{f_1 k_{TT}(1 - P_s)^2 J}{2k_{NR,T}^2 qd}) \tag{8}$$

The prompt fast EL is from the singlet excitons directly formed on TTA molecule, while the delayed slow decay is from the indirect singlets as result of TTA up-conversion process. The delayed emission ratio

$$R_d = \frac{EL_T}{EL_S + EL_T} = \frac{R}{R + 1} = \frac{f_1 k_{TT}(1 - P_s)^2 J}{f_1 k_{TT}(1 - P_s)^2 J + 2k_{NR,T}^2 qdP_s} \tag{9}$$
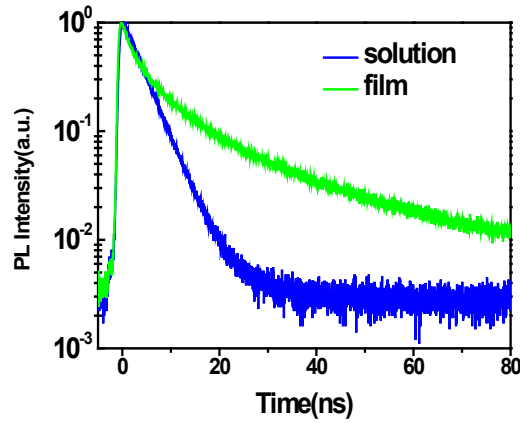
At high current density

$$R = \frac{EL_T}{EL_S} = \frac{f_1(1 - P_s)}{2P_s} \tag{10}$$

$$R_d = \frac{EL_T}{EL_S + EL_T} = \frac{R}{R + 1} = \frac{f_1(1 - P_s)}{f_1(1 - P_s) + 2P_s} \tag{11}$$
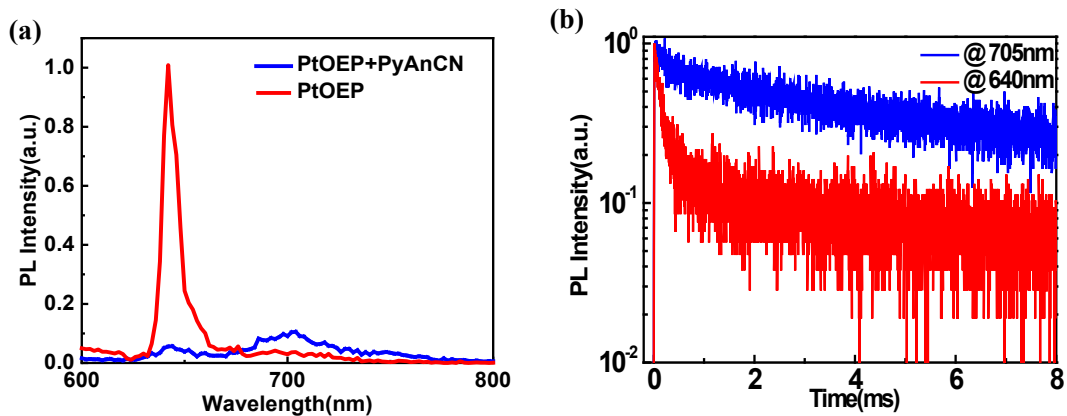
$$EQE = \frac{k_S S \eta_{out}}{\frac{J}{qd}} = \varphi_{PL} \eta_{out} (P_S + \frac{f_1}{2}(1 - P_s)) \tag{12}$$

When the delayed emission ratio at low current density is equal to the delayed emission ratio ,

TTA saturated current density (J_{TTA}) at high current density is as

$$J_{TTA} = \frac{k_{NR,T}^2 qd}{k_{TT}(1 - P_s)} \tag{13}$$

Figure S1. Transient PL decay curves of PyAnCN in toluene solution (10^{-5} M) in air condition and neat film with encapsulation.


Figure S2. (a) Phosphorescence spectra of PtOEP (red) and PyAnCN with PtOEP (blue) in toluene (10^{-5} M, 77K). (b) PL decay curves of PtOEP at 640 nm(red) and PyAnCN with PtOEP at 705 nm (blue) in toluene (10^{-5} M, 77K).
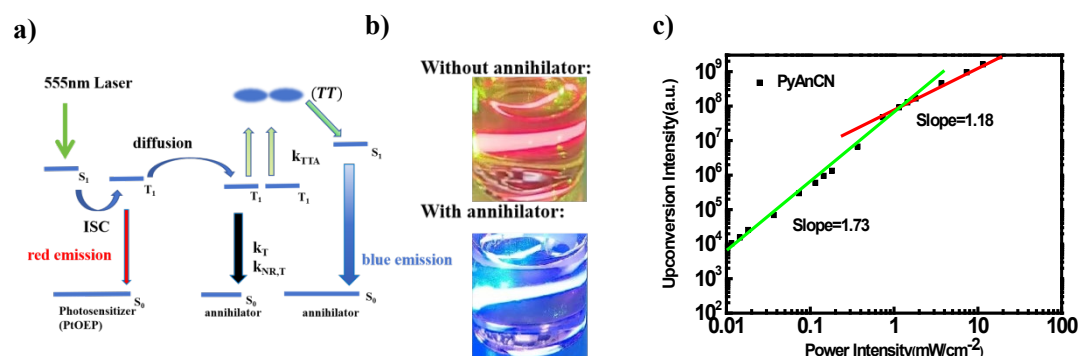
Figure S3. (a) Schematic illustration of the exciton processes in the designed TTA up-conversion system. (b) Photographs of the TTA up-conversion without and with PyAnCN as annihilators, respectively, taken under 5 mW/cm^2 of 555 nm light. (c) Dependence of the TTA up-conversion intensity in the solution of PtOEP and PyAnCN on the various incident power densities. The results fit the lines that have slopes of 1.73 (green, below) and 1.18 (red, above) in the low-power and high-power regions, respectively.
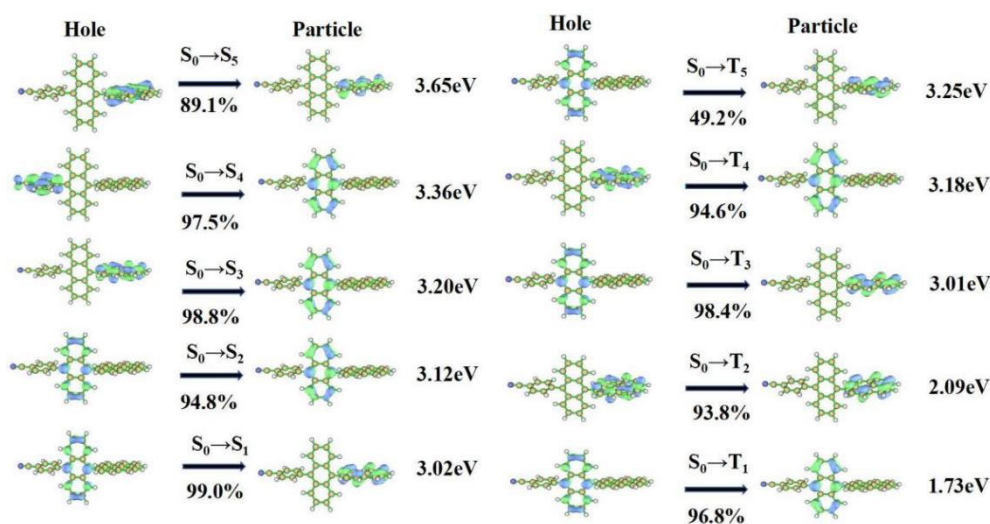
**Figure S4.** NTO transition characters of the singlet and triplet states of PyAnCN.
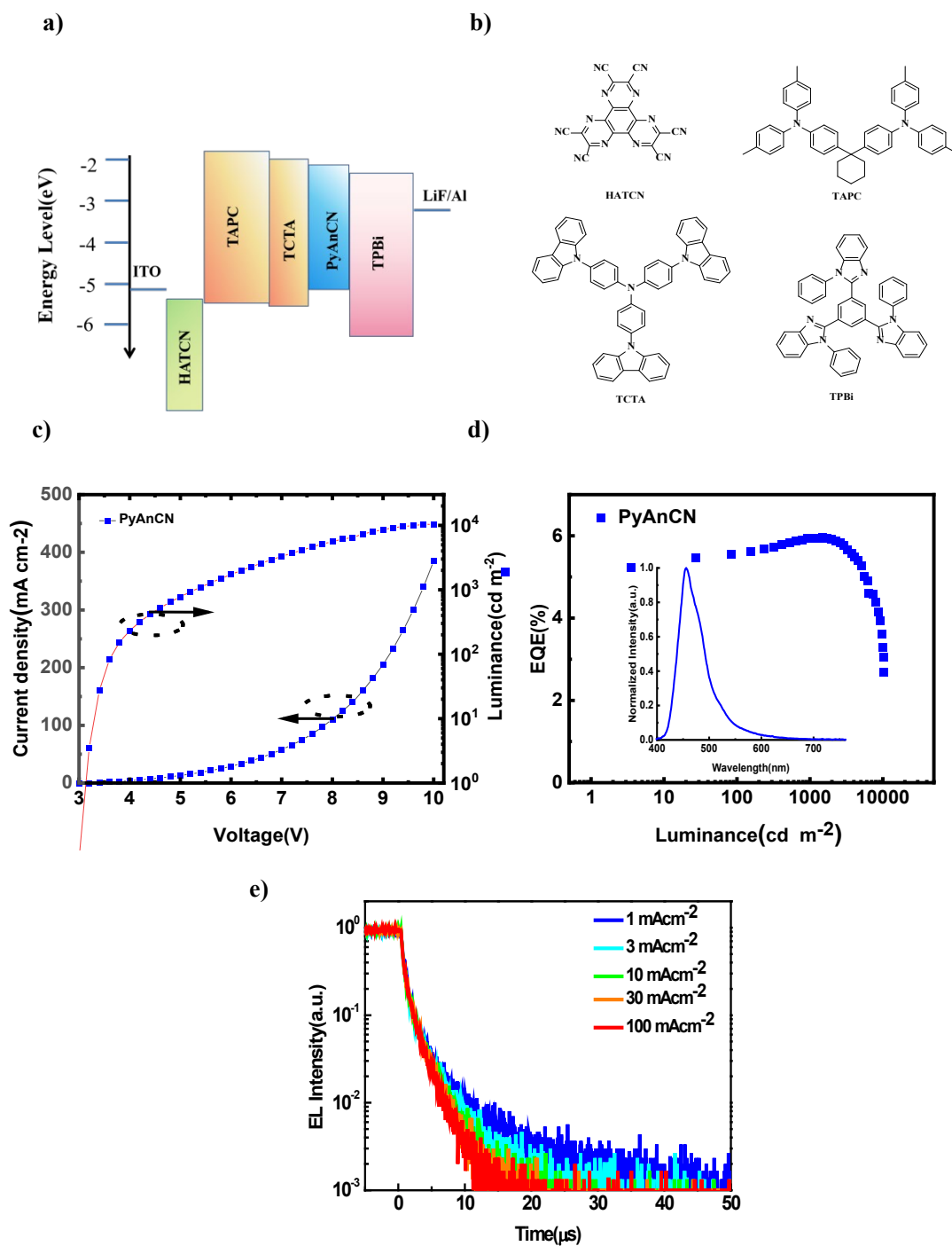
Figure S5. (a) Device structure with energy levels in the resulting non-doped OLED based on PyAnCN. (b) Molecular structures of the materials used in the device. (c) Current density and luminance versus voltage characteristics. (d) EQE versus luminance characteristics. The inset shows the EL spectrum at 6 V. (e)Transient EL decay curves of the non-doped OLED at different current densities.

Table S1. EL performances of the non-doped OLED based on PyAnCN.

Emitter	V_{on}^a(V)	L_{max}^b (cd m^{-2})	$CE_{max}/$ CE_{1000}^c (cd/A)	$EQE_{max}/$ EQE_{1000}^d (%)	EL_{max}^e (nm)	CIE^f (x,y)
PyAnCN	3.2	10392	5.9/5.9	6.0/5.9	450	(0.15,0.11)

a) V_{on}: turn-on voltage at the luminescence of 1 cd m^{-2}. b) L_{max}: maximum luminescence. c) CE_{max}/CE_{1000}: maximum current efficiency/at 1000 cd m^{-2}. d) EQE_{max}/EQE_{1000}: EQE of maximum/at 1000 cd m^{-2}. e) EL_{max}: emission peak of EL spectrum at 6 V. f) CIE coordinates at 6 V.
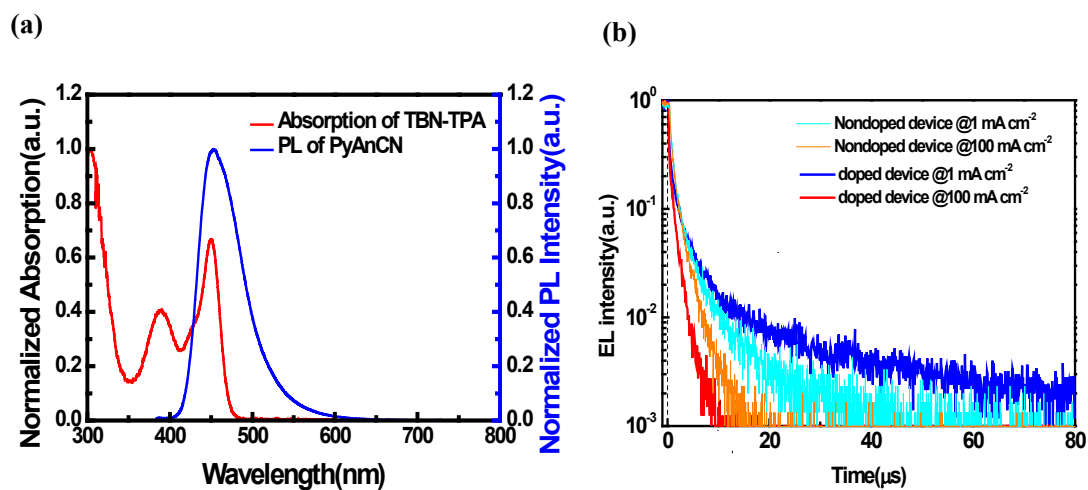
Figure S6. (a) Normalized UV–vis absorption spectrum of TBN-TPA in toluene(10^{-5} M), and PL spectrum of PyAnCN in toluene(10^{-5} M). (b) Comparison of transient EL decay curves of the non-doped (PyAnCN) and doped (PyAnCN:3%TBN-TPA) OLEDs at different current densities.
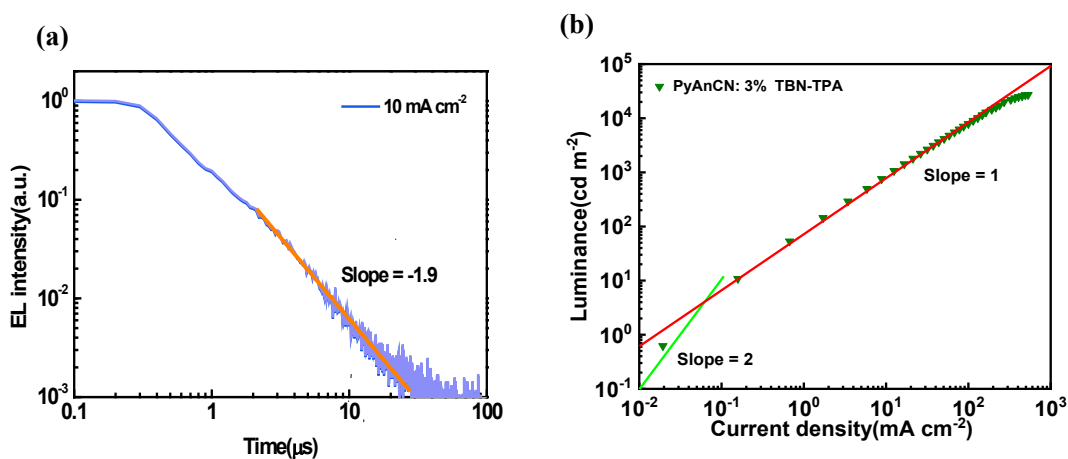
Figure S7. (a) Double-logarithmic EL decay profile in a time range of 2–20 μs in the device based on PyAnCN host (pulse width:100 μs, J = 10 mA cm^{-2}). The red line is the fitting line. (b) luminance as a function of current density for the device based on PyAnCN host.

Table S2. Transient EL parameters fitted by TTA model in OLED based on PyAnCN host at different current densities.

PyAnCN			
J(mAcm^{-2})	A	B	Rd(%)
0.3	0.25	2.31	18.7
1	0.55	1.91	27.4
3	0.83	1.77	31.2
10	1.22	1.65	36.7
30	1.55	1.63	37.6
100	2.11	1.62	38.1

Table S3. Calculated singlet and triplet properties of the first eleven singlet states and twenty triplet states in PyAnCN.

	Singlet states			Triplet states		
	Energy Level(eV)	Oscillator Strength		Energy Level(eV)		Energy Level(eV)
1	3.02	0.0002	1	1.73	12	3.64
2	3.12	0.2628	2	2.09	13	3.74
3	3.20	0.0019	3	3.01	14	3.87
4	3.36	0.0039	4	3.18	15	3.90
5	3.65	0.3170	5	3.25	16	3.95
6	3.74	0.0011	6	3.27	17	4.06
7	3.75	0.0015	7	3.43	18	4.08
8	3.80	0.0000	8	3.44	19	4.14
9	3.94	0.0015	9	3.46	20	4.18
10	4.06	0.0004	10	3.55		
11	4.14	0.0153	11	3.59		

Table S4. Calculated parameter values by the PL decay curves in hosts:3%TBN-TPA films measured in nitrogen.

Host	A_1	t_1(ns)	A_2	t_2(ns)	R_p(%)	R_d(%)
MADN	333	3.9	4.1	51.1	86.2	13.8
PAC	397	5.4	16.1	41.2	76.6	23.4
DMPPP	255	2.9	15.5	42.7	53.2	46.8
PyAnCN	387	3.1	38.9	29.5	51.5	48.5

Table S5. Calculated values of the PL decays by the PL decay curves in hosts:3%TBN-TPA films measured in nitrogen.

| Host	k_S	$k_{NR,S}$	k_{hISC}	k_{hRISC}	PLQY(%)
	$(10^8 s^{-1})$	$(10^7 s^{-1})$	$(10^7 s^{-1})$	$(10^7 s^{-1})$	
MADN	1.7	5.1	8.6	0.9	77
PyAnCN	1.2	5.2	20.8	5.1	69
DMPPP	1.5	3.9	19.4	3.7	82
PAC	1.0	5.0	8.3	1.7	72

The time evolution of singlet and triplet populations in TrPL processes can be modeled for the dual excitation system as

$$\frac{dS}{dt} = I_x - \left(k_S + k_{NR,S}\right)S + k_{hRISC}T_n - k_{hISC}S \qquad ①$$

$$\frac{dT_n}{dt} = k_{hISC}S - (k_{IC} + k_{hRISC})T_n \qquad ②$$

$$\frac{dT_1}{dt} = k_{IC}T_n - k_{NR,T}T_1 \qquad ③$$

I_x represent the exciton generation rate from optical excitation. The optical pulse excitation power was kept at the constant value less than 0.5mW cm^{-2}, so the effect of TTA interaction in the film can be neglected.
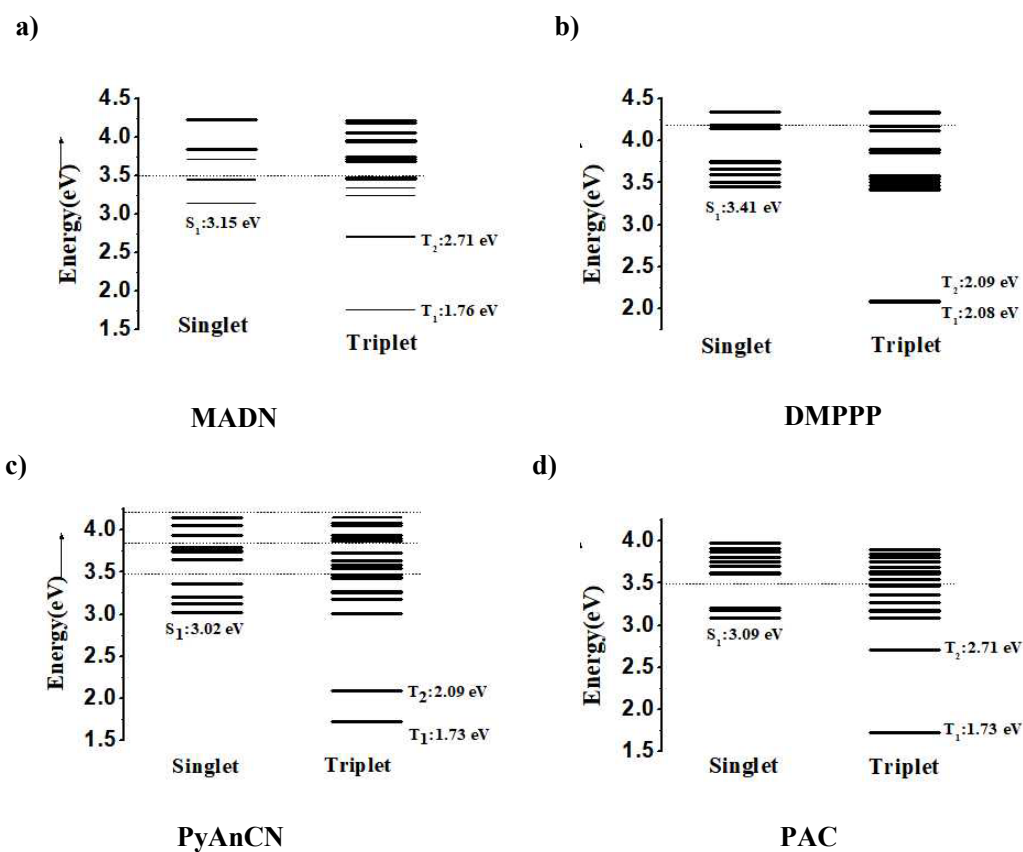
Figure S8. Energy diagrams of the calculated singlet and triplet excited states of MADN, DMPPP, PyAnCN and PAC.

Table S6. Calculated SOC constants between S_1/S_2 and T_n states in **PyAnCN**.

SOC matrix element	[cm^{-1}]	SOC matrix element	[cm^{-1}]
$\langle S_1|\hat{H}_{SOC}|T_1\rangle$	0.0181	$\langle S_2|\hat{H}_{SOC}|T_1\rangle$	0.0755
$\langle S_1|\hat{H}_{SOC}|T_2\rangle$	0.1163	$\langle S_2|\hat{H}_{SOC}|T_2\rangle$	0.1301
$\langle S_1|\hat{H}_{SOC}|T_3\rangle$	0.1206	$\langle S_2|\hat{H}_{SOC}|T_3\rangle$	0.0024
$\langle S_1|\hat{H}_{SOC}|T_4\rangle$	0.0452	$\langle S_2|\hat{H}_{SOC}|T_4\rangle$	0.0013
$\langle S_1|\hat{H}_{SOC}|T_5\rangle$	0.2616	$\langle S_2|\hat{H}_{SOC}|T_5\rangle$	0.1394
$\langle S_1|\hat{H}_{SOC}|T_6\rangle$	0.0776	$\langle S_2|\hat{H}_{SOC}|T_6\rangle$	0.2462
$\langle S_1|\hat{H}_{SOC}|T_7\rangle$	0.3289	$\langle S_2|\hat{H}_{SOC}|T_7\rangle$	0.0337

Table S7. Calculated parameter values by the PL decay curves in PyAnCN:3%TBN-TPA films measured in nitrogen at different temperatures.

Temperature(K)	A_1	t_1(ns)	A_2	t_2(ns)	R_p(%)	R_d(%)	k_{hRISC} $(10^7 s^{-1})$
80	389	2.62	20.5	31.2	61.9	38.1	3.45
130	413	3.08	27.4	32.6	55.7	41.1	3.61
180	400	3.01	31.1	32.2	54.6	45.4	4.14
230	407	3.04	34.6	30.7	53.8	46.2	4.45
280	386	3.07	38.9	29.5	51.5	48.5	5.07

Table S8. Calculated parameter values by the PL decay curves of the PAC:x%PyAnCN:3% TBN-TPA films with different host concentration measured in nitrogen.

| Host	A_1	t_1(ns)	A_2	t_2(ns)	R_p(%)	R_d(%)	k_{hRISC} $(10^7 s^{-1})$
PAC	397	5.4	16.1	41.2	76.6	23.4	1.7
PAC:20%PyAnCN	395	5.2	21.3	39.1	70.9	29.1	2.1
PAC:50%PyAnCN	388	3.1	41.1	29.3	50.9	49.1	5.2
PyAnCN:20%PAC	386	3.1	39.9	28.9	53.8	46.2	5.1
PyAnCN	387	3.1	38.9	29.5	51.1	48.9	5.1
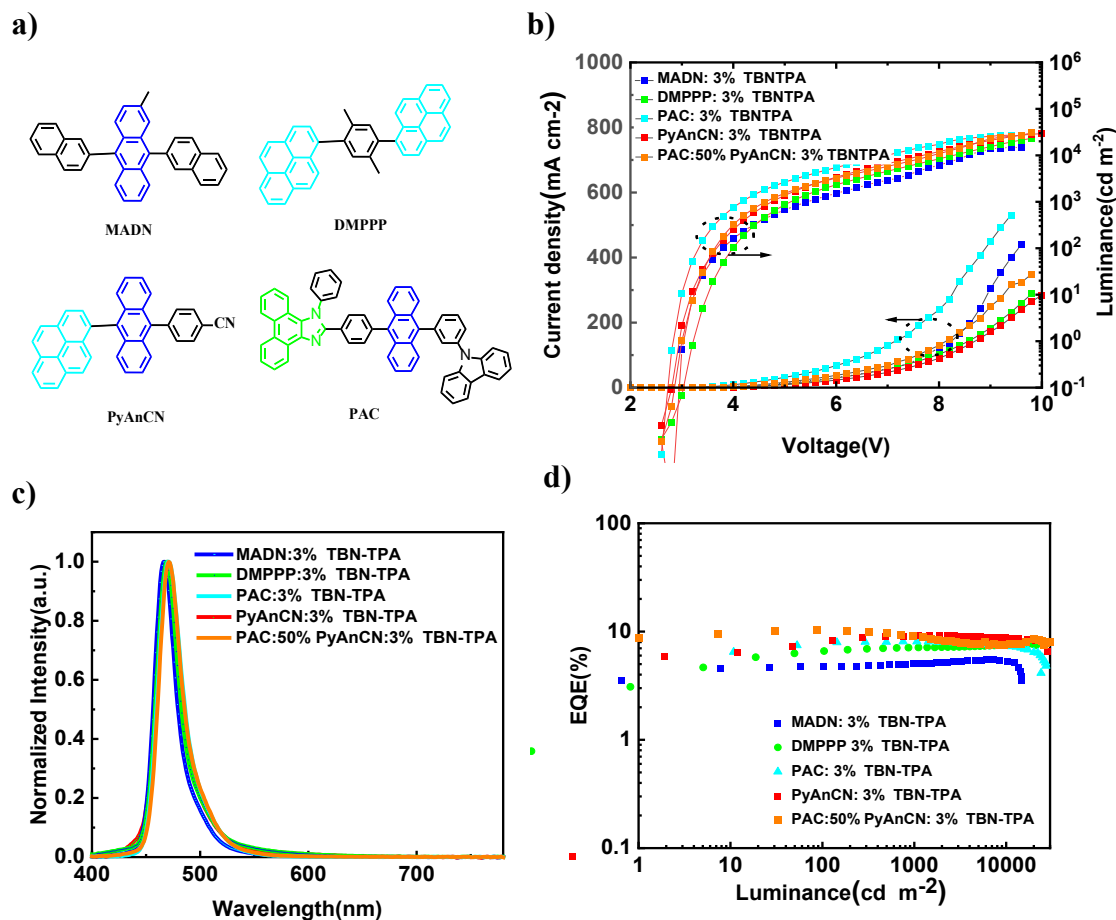
Figure S9. EL performances of the resulting blue OLEDs based on TTA/HLCT hosts. (a) Molecular structures of the materials used in the devices. (b) Current density and luminance versus voltage characteristics. (c) EL spectra at 6 V. (d) EQE versus luminance characteristics.

Table S9. EL performances of the OLEDs based on different EMLs.

EML	V_{on}^a(V)	L_{max}^b(cd m^{-2})	$CE_{max}/CE_{100}{}^c$(cd/A)	$EQE_{max}/EQE_{1000}{}^d$(%)	EL_{max}^e(nm)	CIE^f(x,y)
MADN	3.2	14851	5.3/4.8	5.5/5.0	468	(0.12,0.12)
DMPPP	3.4	25490	8.6/8.0	7.9/7.1	469	(0.14,0.14)
PAC	3	27106	8.6/8.5	8.1/8.0	470	(0.12,0.14)
PyAnCN	3.4	28410	9.7/9.7	9.1/9.1	470	(0.13,0.14)
PAC:50%PyAnCN	3	30286	11.2/11.0	10.3/10.3	470	(0.13,0.14)

a)V_{on}: turn-on voltage at the luminescence of 1 cd m^{-2}; b)L_{max}: maximum luminescence; c)CE_{max}: maximum current efficiency; d)EQE_{max}/EQE_{1000}: EQE of maximum/at 1000 cd m^{-2}; e)EL_{max}: emission peak of EL spectrum at 6 V; f)CIE coordinates at 6 V.
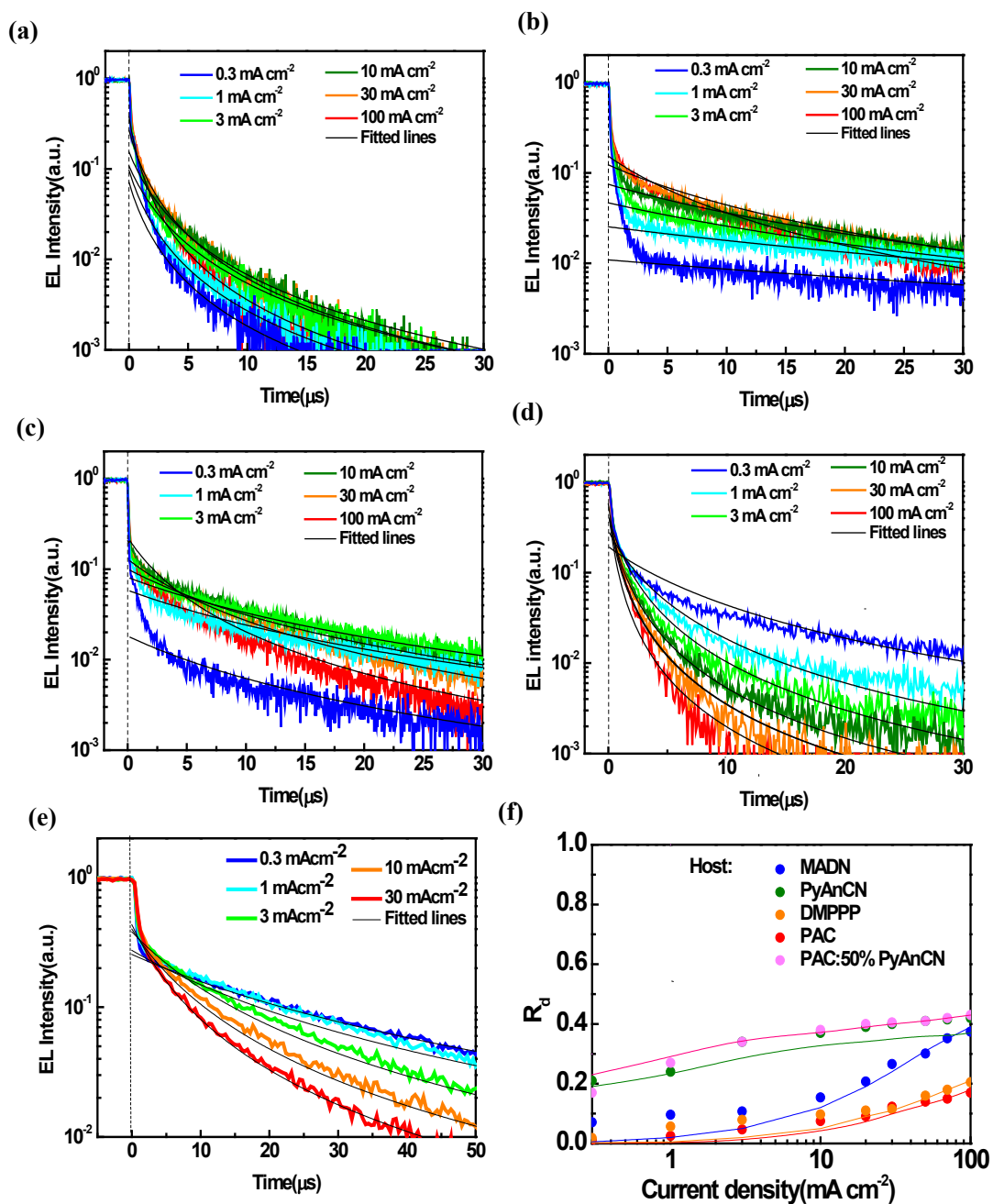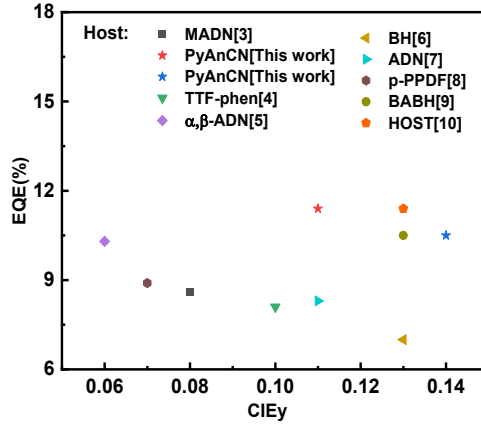
Figure S10. Transient EL decay curves of the resulting hosts:3% TBN-TPA based blue OLEDs (a-e). (a) MADN, (b) PAC, (c) DMPPP, (d) PyAnCN, and (e) PAC:50%PyAnCN. (f) Delayed emission ratio against the current density of hosts:3% TBN-TPA based devices and fitted lines from TTA model.

Table S10. Transient EL parameters fitted by TTA model at different current densities.

MADN				PyAnCN			
$J(mAcm^{-2})$	A	B	Rd(%)	$J(mAcm^{-2})$	A	B	Rd(%)
0.3	1.96	3.75	7.1	0.3	0.25	2.31	18.7
1	1.60	3.22	9.6	1	0.55	1.91	27.4
3	1.05	3.05	10.7	3	0.83	1.77	31.2
10	0.96	2.55	15.4	10	1.22	1.65	36.7
30	1.08	1.94	26.6	30	1.55	1.63	37.6
100	1.31	1.64	37.4	100	2.11	1.62	38.1
DMPPP				PAC			
$J(mAcm^{-2})$	A	B	Rd(%)	$J(mAcm^{-2})$	A	B	Rd(%)
0.3	0.53	7.51	1.8	0.3	0.13	9.57	1.1
1	0.23	4.18	5.7	1	0.13	6.28	2.5
3	0.20	3.55	7.9	3	0.16	4.63	4.7
10	0.25	3.21	9.7	10	0.16	3.66	7.5
30	0.33	2.85	12.3	30	0.19	2.95	11.5
100	0.49	2.21	20.4	100	0.27	2.43	17.1

PAC: 50%PyAnCN			
$J(mAcm^{-2})$	A	B	Rd(%)
0.3	0.054	1.98	25.5
1	0.068	1.91	27.4
3	0.105	1.62	38.1
10	0.15	1.58	40.0
30	0.20	1.52	43.2

Table S11. Calculated values of the PL and EL decays in hosts:3% TBN-TPA films.

Host	k_S	$k_{NR,S}$	k_{hISC}	k_{hRISC}	k_{TT}	$k_{NR,T}$	J_{TTA}	PLQY(%)
	$(10^8 s^{-1})$	$(10^7 s^{-1})$	$(10^7 s^{-1})$	$(10^7 s^{-1})$	$(10^{-14} cm^3 s^{-1})$	$(10^4 s^{-1})$	$(mA\ cm^{-2})$	
MADN	1.7	5.1	8.6	0.9	0.15	9.1	50	77
PyAnCN	1.2	5.2	20.8	5.1	4.1	3.4	0.5	69
DMPPP	1.5	3.9	19.4	3.7	0.02	3.2	7.5	82
PAC	1.0	5.0	8.3	1.7	0.006	2.1	10	72
PAC:50%PyAnCN	1.2	4.3	15.8	6.0	3.9	3.3	0.2	74

Figure S11. Summary of the reported fluorescent OLEDs based on deep blue TTA/HLCT hosts with CIEy < 0.15.

Steady-state kinetic exciton simulation:

The exciton dynamics can be described by the following coupled rate equations as simultaneously considering TTA up-conversion and hRISC of higher triplets:

$$\frac{de}{dt} = \frac{dh}{dt} = \frac{J}{qd} - keh \tag{14}$$

$$\frac{dS}{dt} = P_s keh - (k_S + k_{NR,S})S + \frac{f_1}{2}k_{TT}T_1 T_1 + k_{hRISC}T_n - k_{hISC}S \tag{15}$$

$$\frac{dT_n}{dt} = (1 - P_s)keh - (k_{IC} + k_{hRISC})T_n + k_{hISC}S \tag{16}$$

$$\frac{dT_1}{dt} = k_{IC}T_n - (k_{TT}T_1 + k_{NR,T})T_1 \tag{17}$$

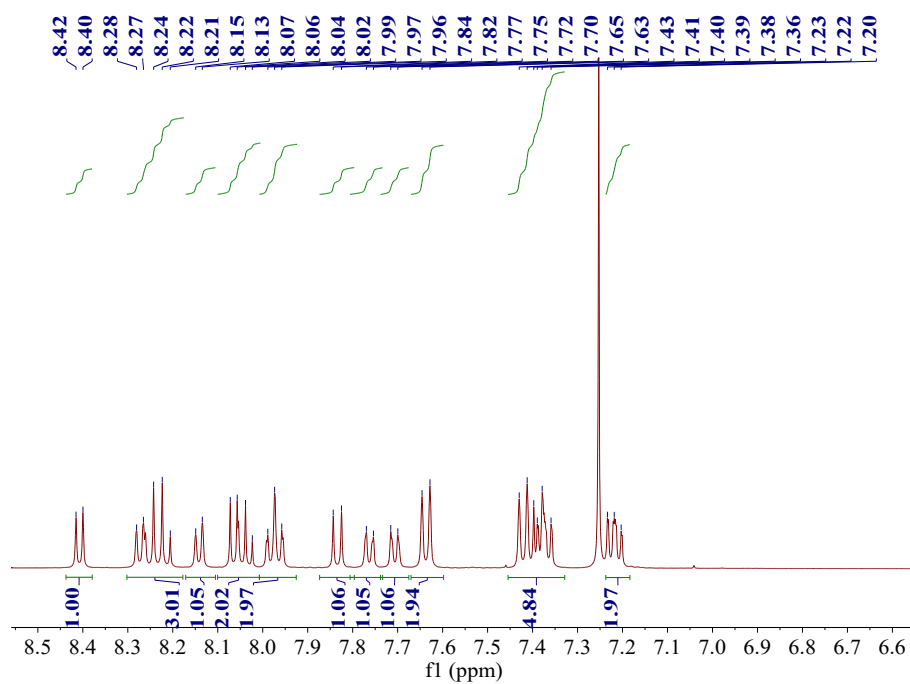$$k = \frac{q(\mu_h + \mu_e)}{\varepsilon_0 \varepsilon_r} \tag{18}$$

k_{hRISC} is the rate of highly-lying reverse intersystem crossing. ε_0 and ε_r is the permittivity of free space and the relative permittivity, respectively. $\mu_h(\mu_e)$ is the hole (electron) mobility of the emissive layer. The width of the recombination zone(d) is assumed as 20 nm, and the hole mobility of the emissive layer is assumed as 1×10^{-6} cm^2 V^{-1}s^{-1} (the electron mobility contributed to the Langevin recombination rate was neglected due to its two orders of magnitude smaller than the hole mobility). The relative permittivity ε_r is assumed as 3. f_1 is assumed as 0.4, and Ps is assumed as 25%. The rate constant of internal conversion processes from T_n to T_1 (k_{IC}) is assumed as same as rate constant of singlet decay. With measured rate constants in PL and EL decay curves, the exciton densities of S, T_2 and T_1 and the delayed emission ratio can be calculated. With calculated concentration of S, T_2 and T_1, the proportion of TTA upconversion(R_{TTA}) is calculated as $(0.2k_{TT}T_1T_1)/(J/ew)$, the proportion of HCLT(R_{HLCT}) is calculated as $((k_SS)/(J/ew)-R_{TTA})$, the proportion of TTA loss($R_{TT, loss}$) channel is calculated as $(0.8k_{TT}T_1T_1)/(J/ew)$, the proportion of non-radiative triplet decay channel is calculated as $(k_{NR,T}T_1)/(J/ew)$, and the proportion of non-radiative singlet decay($R_{NR,S}$) channel is calculated as $(k_{NR,S}S)/(J/ew)$.
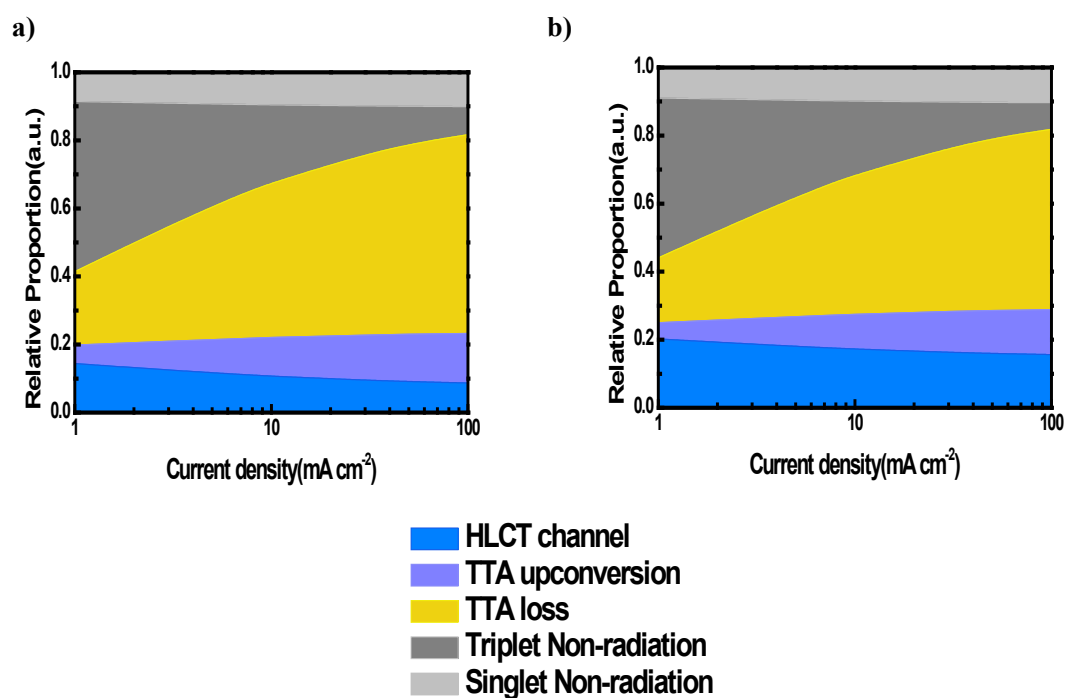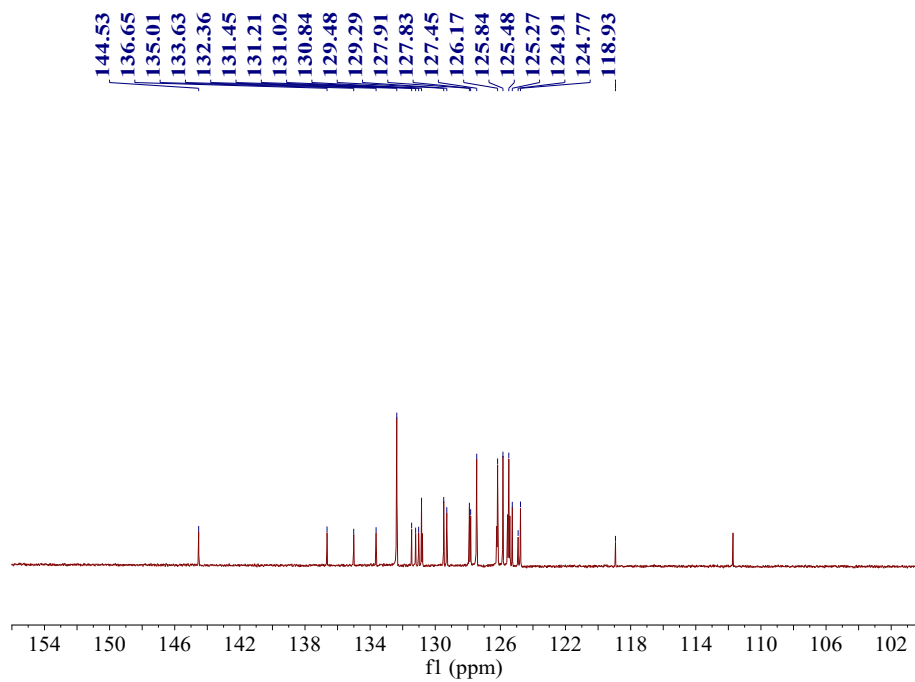

Figure S12. Relative contributions of the different excitonic processes in the resulting blue OLEDs based on different hosts. (a) PyAnCN, (b) PAC: 50%PyAnCN.
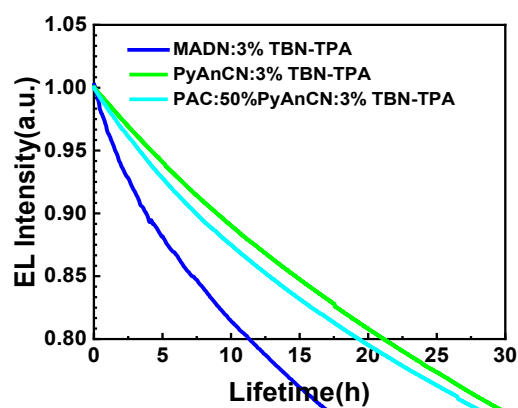
Figure S13. Device lifetime data of ITO/HAT-CN (15 nm)/TAPC (55 nm)/TCTA (10 nm)/MADN or PyAnCN and PAC:50%PyAnCN:3%TBN-TPA (20 nm)/TPBi (40 nm)/LiF (1 nm)/Al at 30 mA cm^{-2}.
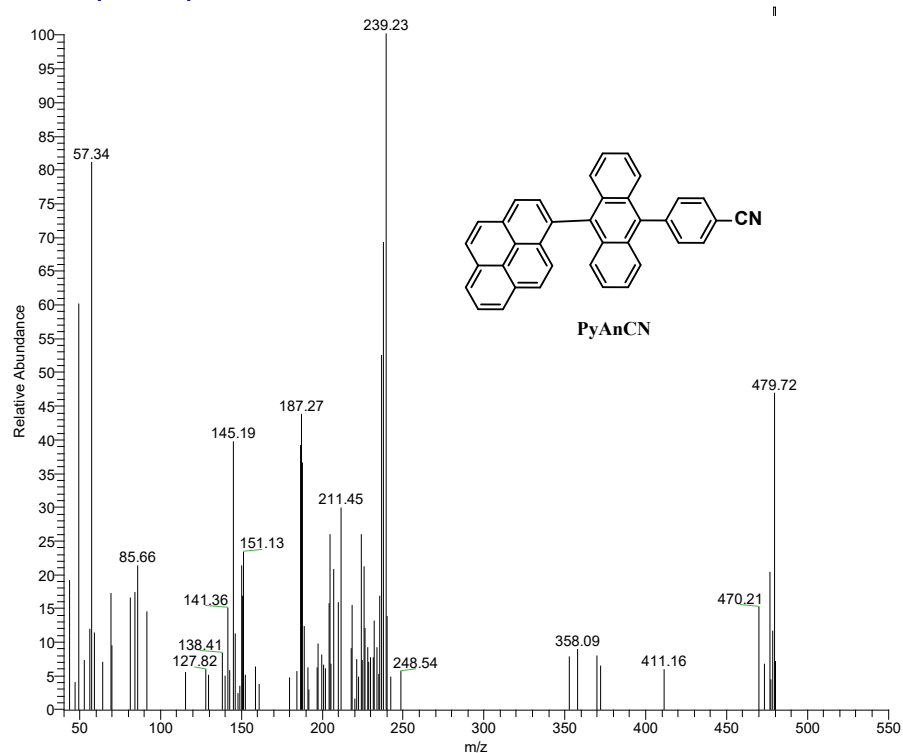

Figure S14. ^{1}H NMR spectra of PyAnCN.

144.53 136.65 135.01 133.63 132.36 131.45 131.21 131.02 130.84 129.48 129.29 127.91 127.83 127.45 126.17 125.84 125.48 125.27 124.91 124.77 118.93

Figure S15. ^{13}C NMR spectra of PyAnCN.

Q1 #338   RT: 5.90   AV: 1   SB: 241 0.51-4.59 , 6.23-6.30   NL: 8.65E2
T: + c Full ms [40.00-550.00]

Figure S16. Mass spectra of PyAnCN.

References

[1] X. Tang, Q. Bai, T. Shan, J. Li, Y. Gao, F. Liu, H. Liu, Q. Peng, B. Yang, F. Li and P. Lu, *Adv. Funct. Mater.* 2018, **28**, 1705813.

[2] C. Lin, P. Han, S. Xiao, F. Qu, J. Yao, X. Qiao, D. Yang, Y. Dai, Q. Sun, D. Hu, A. Qin, Y. Ma, B. Z. Tang, D. Ma, *Adv. Funct. Mater.* 2021, **31**, 202106912.

[3] H. Lim, S. J. Woo, Y. H. Ha, Y. H. Kim and J. J. Kim, *Adv. Mater.* 2022, **34**, e2100161.

[4] J. Lim, J. M. Kim, J. Y. Lee, *Adv.Mater.* 2024, e2312774.

[5] X. Wang, L. Wang, G. Meng, X. Zeng, D. Zhang, L. Duan, *Sci. Adv.* 2023, **9**, eadh1434.

[6] Z. Wang, Z. Yan, Q. Chen, X. Song, J. Liang, K. Ye, Z. Zhang, H. Bi, Y. Wang, *ACS Appl. Mater. Interfaces.* 2023, **15**, 14605.

[7]T. B. Nguyen, H. Nakanotani, C. Y. Chan, S. Kakumachi, C. Adachi, *ACS Appl. Mater. Interfaces.* 2023, **15**, 23557.

[8] S. Hyun Lee, M. Young Chae, Y. Hun Jung, J. Hyeog Oh, H. Rin Kim, K. R. Naveen, J. H. Kwon, *J. Ind. Eng. Chem.* 2023, **122**, 452.

[9] C. Kuang, S. Li, I. Murtaza, Z. Meng, H. Li, X. Zhang, C. Wu, K. N. Tong, Y. Shang, Y. He, Y. Zhu, G. Wei, H. Meng, *Small.* 2023, e2311114.

[10] J. Park, K. J. Kim, J. Lim, T. Kim, J. Y. Lee, *Adv.Mater.* 2022, **34**, e2108581.